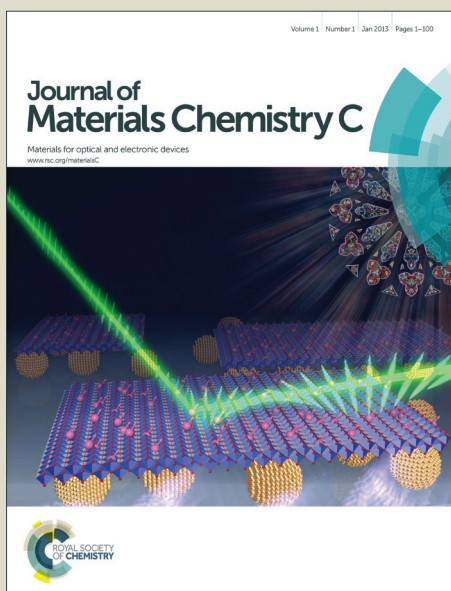


# Journal of Materials Chemistry C

Accepted Manuscript



This is an *Accepted Manuscript*, which has been through the Royal Society of Chemistry peer review process and has been accepted for publication.

*Accepted Manuscripts* are published online shortly after acceptance, before technical editing, formatting and proof reading. Using this free service, authors can make their results available to the community, in citable form, before we publish the edited article. We will replace this *Accepted Manuscript* with the edited and formatted *Advance Article* as soon as it is available.

You can find more information about *Accepted Manuscripts* in the [Information for Authors](#).

Please note that technical editing may introduce minor changes to the text and/or graphics, which may alter content. The journal's standard [Terms & Conditions](#) and the [Ethical guidelines](#) still apply. In no event shall the Royal Society of Chemistry be held responsible for any errors or omissions in this *Accepted Manuscript* or any consequences arising from the use of any information it contains.



## Tunable green-yellowish-orange phosphor $\text{Na}_3\text{LuSi}_2\text{O}_7:\text{Eu}^{2+}, \text{Mn}^{2+}$ via energy transfer for UV-LEDs

Kai Li,<sup>ab</sup> Mengjiao Xu,<sup>a</sup> Jian Fan,<sup>a</sup> Mengmeng Shang,<sup>a</sup> Hongzhou Lian<sup>\*a</sup> and Jun Lin<sup>\*a</sup>

Received 00th January 20xx,  
Accepted 00th January 20xx

DOI: 10.1039/x0xx00000x

www.rsc.org/

A series of  $\text{Eu}^{2+}$ ,  $\text{Mn}^{2+}$ -doped  $\text{Na}_3\text{LuSi}_2\text{O}_7$  (NLSO) phosphors have been prepared via the high-temperature solid-state reaction route. X-ray diffraction (XRD), Raman and Fourier transform infrared (FT-IR) spectra, fluorescent decay times, photoluminescence (PL) including temperature-dependent PL properties, scanning electron microscope (SEM) were used to characterize the as-prepared samples. In  $\text{Eu}^{2+}$  singly-doped NLSO samples, they presented intense green emission under UV excitation. The tunable color from green to yellowish-orange was generated when  $\text{Mn}^{2+}$  ions were co-doped into the  $\text{NLSO}:\text{Eu}^{2+}$ , which is based on the energy transfer from  $\text{Eu}^{2+}$  to  $\text{Mn}^{2+}$  ions. The energy transfer property from  $\text{Eu}^{2+}$  to  $\text{Mn}^{2+}$  ions can be speculated by the wide spectral overlap between  $\text{Eu}^{2+}$  emission and  $\text{Mn}^{2+}$  excitation spectra in  $\text{Eu}^{2+}$  or  $\text{Mn}^{2+}$  singly doped NLSO samples and demonstrated by the similar excitation spectra of  $\text{Eu}^{2+}$  and  $\text{Mn}^{2+}$  ions emission bands and the decreases of  $\text{Eu}^{2+}$  emission intensity and decay lifetimes with the raise of  $\text{Mn}^{2+}$  concentration in  $\text{NLSO}:\text{Eu}^{2+}, \text{Mn}^{2+}$  samples. The energy transfer mechanism from  $\text{Eu}^{2+}$  to  $\text{Mn}^{2+}$  ions was determined to be dipole-quadrupole interaction by the concentration quenching and spectral overlap methods. The maximum quantum yield can reach 51.5% for  $\text{NLSO}:0.01\text{Eu}^{2+}, 0.12\text{Mn}^{2+}$ . The above results indicate that  $\text{NLSO}:\text{Eu}^{2+}, \text{Mn}^{2+}$  can be a candidate as a green-yellowish-orange component for UV-excited w-LEDs.

### 1 Introduction

Currently, energy saving has been a global tactics to dispose the energy shortage issue we have to face. Phosphor conversion white light-emitting diodes (w-LEDs) have been considered to be the next generation solid-state lighting systems to replace the current traditional fluorescent and incandescent lamps due to their unique advantages such as long operational lifetime, high efficiency, compactness, low energy consumption and free from toxicity.<sup>1</sup> Therefore, they have been drawn increasing attention. Lacking red component in the usual w-LEDs which are often realized by employing the yellow phosphor  $\text{YAG}:\text{Ce}^{3+}$  with a blue  $\text{InGaN}$  LED chip arouses a lot of problems especially containing a poor color-rendering index (CRI) and high correlated color temperature (CCT), limiting their use in more vivid applications.<sup>2</sup> Therefore, coating tricolor (blue/green/red) phosphors on UV/n-UV LED chips has been an attractive method to realize the warm white light with high color uniformity and CRI, which would be anticipated to occupy the market in the near future.<sup>3</sup> As the indispensable component, the new phosphors excited by the UV/n-UV radiation are attracting increasing attention, which makes it a hot research topic in the phosphors field. Consequently, exploring different tricolor phosphors is of great importance to meet the forthcoming demand

in the fabrication process of w-LED. As we know, there are many reports related to the development of tri-color emission phosphors, in which they often introduce  $\text{Eu}^{2+}$  or  $\text{Ce}^{3+}$  as the activator(s) because both two rare earth ions are sensitive to the crystal field and covalence since their 4f-5d transition are spin-allowed, generally presenting superior absorption bands in the spectral region of 250–450 nm to match well with UV/n-UV chips, such as  $\text{Ca}_2\text{GdZr}_2(\text{AlO}_4)_3:\text{Ce}^{3+}$ ,  $\text{Ca}_{1.4}\text{Al}_{2.8}\text{Si}_{9.2}\text{N}_{16}:\text{Ce}^{3+}, \text{Li}^+$ ,  $\text{Na}_x\text{Ca}_{1-x}\text{Al}_{2-x}\text{Si}_{2+x}\text{O}_8:\text{Eu}^{2+}$ ,  $\text{Ba}_2\text{Y}_3[\text{SiO}_4]_3\text{F}:\text{Ce}^{3+}$ ,  $\text{Ba}_3\text{Si}_6\text{O}_{12}\text{N}_2:\text{Eu}^{2+}$ .<sup>4</sup> However,  $\text{Eu}^{2+}$  and  $\text{Ce}^{3+}$  also can be as the sensitizers to transfer their energy to  $\text{Mn}^{2+}$ , which often can produce orange or red color based on its spin-forbidden 3d-3d absorption transitions, thus enhancing its weak emission and generating tunable color attributed to the energy transfer effect from  $\text{Eu}^{2+}$  or  $\text{Ce}^{3+}$  to  $\text{Mn}^{2+}$  ions.<sup>5</sup>

Since the number of the existing silicate compounds is large with many kinds of crystal structures. In addition, they possess many alluring features such as mechanical, good thermal, chemical and physical stabilities owing to their strong and rigid frameworks with covalent Si-O bonds.<sup>6</sup> Thereby, they may make them be usefully utilized as the hosts for doping rare earth ions to obtain many kinds of phosphors for the field of solid-state lighting. Some related phosphors have been reported, such as  $\text{Ca}_3\text{Si}_2\text{O}_7:\text{Eu}^{2+}$ ,  $\text{Ba}_2\text{MgSi}_2\text{O}_7:\text{Eu}^{2+}$ ,  $\text{Na}_2\text{Ca}_3\text{Si}_6\text{O}_{16}:\text{Eu}^{2+}$ ,  $\text{Ca}_3\text{SnSi}_2\text{O}_9:\text{Bi}^{3+}, \text{Dy}^{3+}, \text{Eu}^{3+}$ ,  $\text{Mg}_2\text{Al}_4\text{Si}_5\text{O}_{18}:\text{Dy}^{3+}$ .<sup>7</sup> Recently, Xia and Chen group<sup>8</sup> have developed novel  $\text{Eu}^{2+}$ -doped  $\text{NaBaScSi}_2\text{O}_7$  and  $\text{NaBa}(\text{Y}, \text{Sc})\text{Si}_3\text{O}_9$ , and  $\text{KSrScSi}_2\text{O}_7$  phosphors, respectively, which present good performance in photoluminescence (PL) properties. This inspires us that the introduction of Sc element in silicates would be stable for the doping of rare earth ions. However, the silicate compounds containing Lu element whose atom radius is closest to Sc in rare

<sup>a</sup>State Key Laboratory of Rare Earth Resource Utilization, Changchun Institute of Applied Chemistry, Chinese Academy of Sciences, Changchun 130022, P. R. China. Email: jlin@ciac.ac.cn (Jun Lin); hzlian@ciac.ac.cn (Hongzhou Lian) Fax: +86-431-85698041; 86-431-85262031

<sup>b</sup>University of Chinese Academy of Sciences, Beijing 100049, P. R. China.

earth elements are rarely regarded as the hosts for doping of rare earth ions. This kind of silicate compounds also may be appropriate for rare earth ions doping and would like to generate good PL properties under UV/n-UV radiation. Therefore, we explore to obtain some Lu-involved silicate and incorporate some rare earth ions into them. After some failures, we synthesize the novel  $\text{Eu}^{2+}$  and  $\text{Eu}^{2+}$ ,  $\text{Mn}^{2+}$  co-doped  $\text{Na}_3\text{LuSi}_2\text{O}_7$  phosphors, producing the intense tunable color from green to yellowish-orange excited under UV light, different from that of previous  $\text{Ce}^{3+}$ -doped  $\text{Na}_3\text{LuSi}_2\text{O}_7$ .<sup>9</sup> In this paper, the structure, PL properties and the crystallographic occupancy of  $\text{Eu}^{2+}/\text{Mn}^{2+}$  in the  $\text{Na}_3\text{LuSi}_2\text{O}_7$  matrix are investigated in detail. The results suggest that it would be recognized as a promising green to yellowish orange phosphor for UV w-LEDs.

## 2 Experimental

### 2.1 Materials and Preparation

The objective products with the stationary chemical composition  $\text{Na}_{3-x}\text{LuSi}_2\text{O}_7:x\text{Eu}^{2+}$  and  $\text{Na}_{2.99}\text{Lu}_{1-y}\text{Si}_2\text{O}_7:0.01\text{Eu}^{2+},y\text{Mn}^{2+}$  (abbreviated as  $\text{NLSO}:x\text{Eu}^{2+}$  and  $\text{NLSO}:0.01\text{Eu}^{2+},y\text{Mn}^{2+}$ ;  $x = 0-0.07$  and  $y = 0.01-0.12$  are the mole dopant concentration) were synthesized via the high-temperature solid-state reaction method. The  $\text{Na}_2\text{CO}_3$  (A.R.),  $\text{SiO}_2$  (A.R.),  $\text{MnCO}_3$  (A.R.),  $\text{Lu}_2\text{O}_3$  (99.99%) and  $\text{Eu}_2\text{O}_3$  (99.99%), without any purity, were regarded as the raw materials. In a typical process, the starting materials were weighed according to the given mole ratio and blended with each other by grinding them in an agate mortar with proper ethanol addition, after which the mixture was placed into the crucible and transformed to the tube furnace to sinter at 1200 °C for 8 h to gain the final samples under 20% $\text{H}_2$ /80% $\text{N}_2$  atmosphere condition followed by reground for 1 min. The 20% $\text{H}_2$ /80% $\text{N}_2$  atmosphere was chosen to complete the reduction of  $\text{Eu}^{2+}$  in NLSO samples. After calcination, the samples were furnace-cooled to room temperature with continuous reductive current, and then crushed again into powders for the subsequent characterization.

### 2.2 Measurement and Characterization

All measurements were conducted using the finely ground powder. The phase purity of samples was analyzed by D8 Focus diffractometer at a scanning rate of  $10^\circ\text{min}^{-1}$  in the  $2\theta$  range from  $10^\circ$  to  $100^\circ$  with graphite-monochromatized  $\text{Cu K}\alpha$  radiation ( $\lambda = 0.15405$  nm). Infrared spectra were collected on a VERTEX 70 Fourier transform infrared (FT-IR) spectrometer (Bruker). Raman spectrum was detected on the Reinshaw micro-Raman spectrometer (equipped with a 514.5 nm Ar+ laser as an excitation source). The morphology of the sample was inspected using a scanning electron microscope (SEM, S-4800, Hitachi). The Hitachi F-7000 spectrophotometer equipped with a 150 W xenon lamp as the excitation source was used to carry out the photoluminescence (PL) measurements, and the diffuse reflectance spectra were gained using a Hitachi U-4100 spectrophotometer with the reflection of black felt (reflection 3%) and white  $\text{BaSO}_4$  (reflection 100%) which was used as a reference standard. The luminescence decay lifetimes were measured and obtained from a Lecroy Wave Runner 6100 Digital Oscilloscope (1 GHz) using a tunable laser (pulse width = 4 ns, gate = 50 ns) as the excitation (Continuum Sunlite OPO) source. PL quantum yields (QYs) of phosphors were obtained directly by the

absolute PL quantum yield measurement system (C9920-02, Hamamatsu Photonics K. K., Japan). All the above measurements were performed at room temperature (RT). Furthermore, the temperature-dependent (298-523 K) PL spectra were measured on a fluorescence spectrophotometer equipped with a 450 W xenon lamp as the excitation source (Edinburgh Instruments FLSP-920) and a temperature controller.

## 3 Results and Discussion

### 3.1 Structure and phase purity

Fig. 1 shows the Rietveld analysis of powder XRD profiles of the representative NLSO host and  $\text{NLSO}:0.005\text{Eu}^{2+}$  samples conducted by the general structure analysis system (GSAS) method, in which the red solid lines, black crosses, olive lines and orange bars are calculated patterns, experimental patterns, differences and Bragg position, respectively. The structural parameters from the  $\text{Na}_3\text{LuSi}_2\text{O}_7$  structure (ICSD 65344) are employed as the initial model. The final refined results of NLSO and  $\text{NLSO}:0.005\text{Eu}^{2+}$  are shown in Table 1. The weighted profile R-factor ( $R_{wp}$ ) and the expected R factor ( $R_p$ ) are 5.09% and 3.75%, and 5.58% and 3.65%, respectively, for NLSO and  $\text{NLSO}:0.005\text{Eu}^{2+}$ , which indicate that as-prepared two samples crystallize with pure phases. Detailed information can be found in Table 1. The crystallinity and purity of the series of as-prepared  $\text{NLSO}:x\text{Eu}^{2+}$  ( $x = 0, 0.005$  and  $0.03$ ) and  $\text{NLSO}:0.01\text{Eu}^{2+}, 0.09\text{Mn}^{2+}$  compounds were examined by X-ray powder diffraction (XRD), which are displayed in Fig. 2. The XRD profiles of as-prepared samples are well assigned to the standard reference of hexagonal  $\text{Na}_3\text{LuSi}_2\text{O}_7$  (JCPDS79-0421), and no any traces of impurity phases are observed, which indicates single phase NLSO phosphors have been obtained, and doping  $\text{Eu}^{2+}$  into this host produce little impurity or induce any significant change to crystal structure. We propose that the close ionic radii between  $\text{Eu}^{2+}$  [ $r = 1.17$  Å for coordination number (CN = 6),  $1.07$  Å for CN = 3,  $1.10$  Å for CN = 4] and  $\text{Na}^+$  ( $1.02$  Å for CN = 6,  $0.98$  Å for CN = 3,  $0.99$  Å for CN = 4) ions suggest that  $\text{Eu}^{2+}$  would accommodate  $\text{Na}^+$  sites in this kind of host, which is considered to be reasonable from the refinement of  $\text{NLSO}:0.005\text{Eu}^{2+}$  above. And the  $\text{Lu}^{3+}$  would like to be substituted by  $\text{Mn}^{2+}$  in  $\text{NLSO}:\text{Eu}^{2+}$ ,  $\text{Mn}^{2+}$  samples, which is also based on the close radii between  $\text{Mn}^{2+}$  ( $r = 0.83$  Å, CN=6) and  $\text{Lu}^{3+}$  ( $r = 0.86$  Å, CN=6) ions. The NLSO compound was first reported by Tamazyan, R. A. et al. in 1988,<sup>10</sup> which has the hexagonal structure similar with space group of P63/m and cell parameters  $a = 9.385$  Å,  $b = 9.385$  Å,  $c = 13.716$  Å,  $Z = 6$  and  $V = 1046.23$  Å<sup>3</sup>. Fig. 3 presents the stereo unit cell and two-direction views of NLSO structure, as well as the different coordination environments of  $\text{Na}^+$  in this structure. There are four distinct  $\text{Na}^+$  lattice sites in NLSO, defined as Na1, Na2, Na3 and Na 4. They locate at Wyck. 2b, 2d, 2c and 12i sites with the corresponding coordination oxygen atoms of six, three, six and four, respectively. The selected Na-O bond lengths are listed in Table 2, For Na1 octahedron, six Na1-O3 share the same bond length (2.557 Å). Two Na2-O4 have the same bond length 2.248 Å and one Na2-O4 2.247 Å with the average bond length of 2.248 Å. Six Na3-O2 share the same bond length of 2.508 Å. Na4-O1, Na4-O1, Na4-O2 and Na4-O3 have the bond length of 2.354 Å, 2.536 Å, 2.343 Å and 2.315 Å with the average bond length of 2.387 Å, respectively.

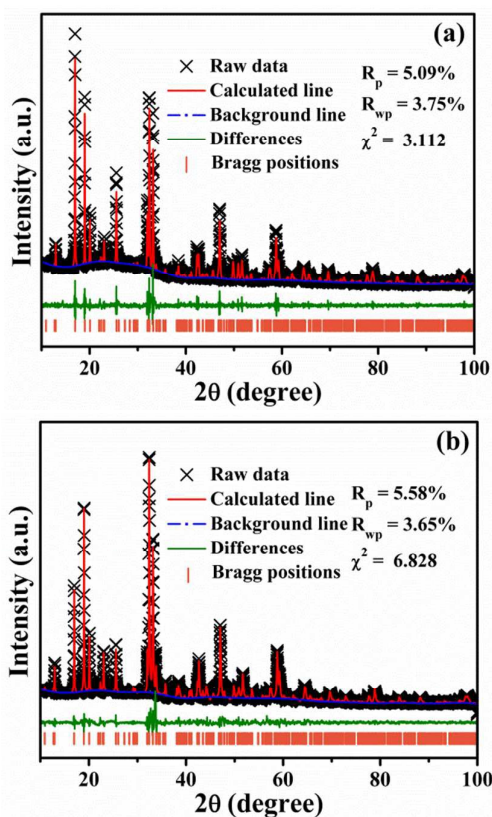


**Fig. 1** Rietveld refinement of powder XRD profiles of the representative NLSO host (a) and NLSO:0.005Eu<sup>2+</sup> (b) samples.

The Raman spectrum of Na<sub>3</sub>LuSi<sub>2</sub>O<sub>7</sub> is displayed in Fig. 4. Several bands in the low-, mid-, and high-wavenumber extent were recorded. Symmetric Si-O stretching vibrations of SiO<sub>4</sub> groups with nonbridging oxygens emerge in alkali silicates with different contents of metal oxides in the high wavenumber range 850-1250 cm<sup>-1</sup>.<sup>11</sup> The peaks here at 861, 942, 961 cm<sup>-1</sup> are attributed to the symmetric ν<sub>3</sub>(Si-O) stretching vibration of the Si<sub>2</sub>O<sub>7</sub> groups, which is consistent with other silicates containing disilicate groups.<sup>12</sup> In the literature, the Raman shifts in the range between 710 and 610 cm<sup>-1</sup> were usually ascribed to the symmetric stretching vibration ν<sub>3</sub>(Si-O-Si) of Si<sub>2</sub>O<sub>7</sub> groups, bending vibrations of the Si-O-Si bridging

**Table 1** Crystallographic data and details in the data collection and refinement parameters for the NLSO and NLSO:0.005Eu<sup>2+</sup> samples.

Sample	NLSO	NLSO:0.005Eu <sup>2+</sup>
Space group	<i>P63/m</i>	<i>P63/m</i>
Symmetry	hexagonal	hexagonal
a, Å	9.3524(1)	9.3573(1)
b, Å	9.3524(1)	9.3573(1)
c, Å	13.6765 (3)	13.6862 (3)
V, Å <sup>3</sup>	1036.00(3)	1037.80(4)
Z	6	6
2θ-interval, °	10-100	10-100
R <sub>p</sub>	3.75	3.65
R <sub>wp</sub>	5.09	5.58
χ <sup>2</sup>	3.112	6.828

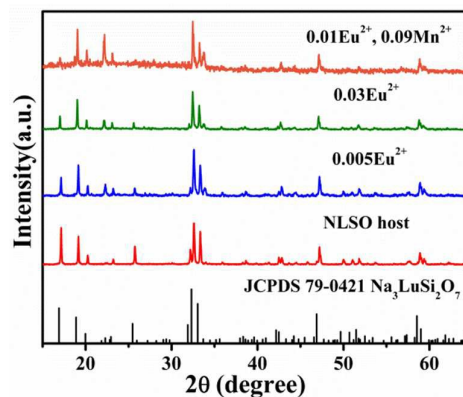


**Fig. 2** The powder XRD patterns of the representative NLSO host, NLSO:0.005Eu<sup>2+</sup>, NLSO:0.03Eu<sup>2+</sup>, NLSO:0.01Eu<sup>2+</sup>,0.09Mn<sup>2+</sup>, as well as the standard reference of Na<sub>3</sub>LuSi<sub>2</sub>O<sub>7</sub> (JCPDS 79-0421).

oxygens between adjacent SiO<sub>4</sub> tetrahedra.<sup>13</sup> According to Galuskin et al.<sup>14</sup> this region consists of a band at 710 cm<sup>-1</sup> (theoretical mode) which is aroused by a properly stretching (Si-O) or as bending (O-Si-O) vibration of Si<sub>2</sub>O<sub>7</sub> groups. In lutecium orthosilicate compounds, vibration bands in the 500-700 cm<sup>-1</sup> range are generally characteristic for the LuO<sub>6</sub> octahedra, which occur in this crystal structure. Below 400 cm<sup>-1</sup>, bands are primarily caused by lattice vibrations of the framework and sodium-oxygen bonding.

The FT-IR spectra of the NLSO host and Eu<sup>2+</sup>-doped samples with different doping concentration have been presented in Fig. 5. It is clearly seen the obtained profiles of FT-IR spectra of Eu<sup>2+</sup>-doped samples are similar to NLSO host, which indicates the accommodation of Eu<sup>2+</sup> into this host has the little change to the structure of the NLSO, agreeing with the XRD analysis above. The peaks around 872 and 936 cm<sup>-1</sup> in 800 to 1200 cm<sup>-1</sup> are indexed to asymmetric Si-O stretching modes of the SiO<sub>4</sub> tetrahedron, while the sharp peaks in mid-frequency range from 600 to 800 cm<sup>-1</sup> including obvious 698 cm<sup>-1</sup> here can be attributed to Si-O-Si bending mode as well as symmetric O-Si-O stretching vibrations in [Si<sub>2</sub>O<sub>7</sub>]<sup>6-</sup> group,<sup>15</sup> which has been demonstrated in Raman spectra above. Another two long absorption peaks of FT-IR spectra at about 1640 and 3437 cm<sup>-1</sup> are assigned to the OH<sup>-</sup> stretching vibrations mode originating from the covered water on the surface of samples under air condition.

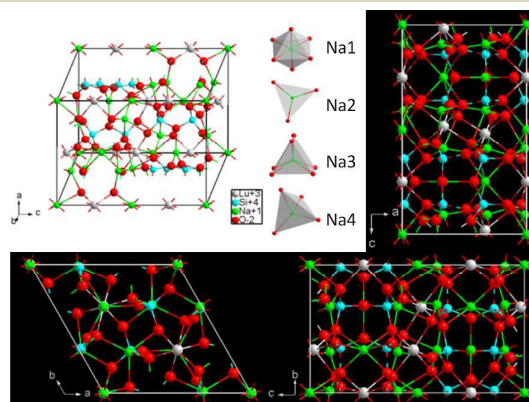


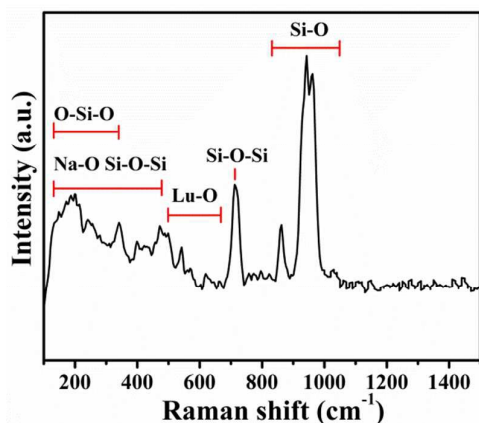
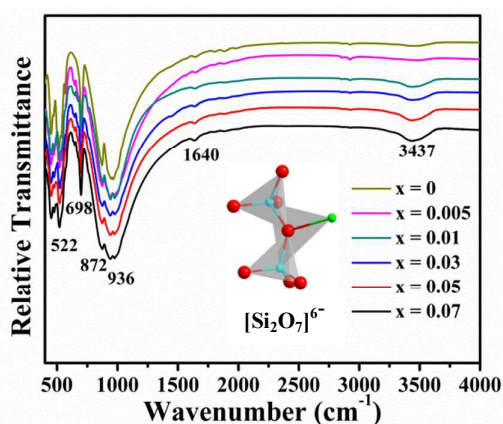
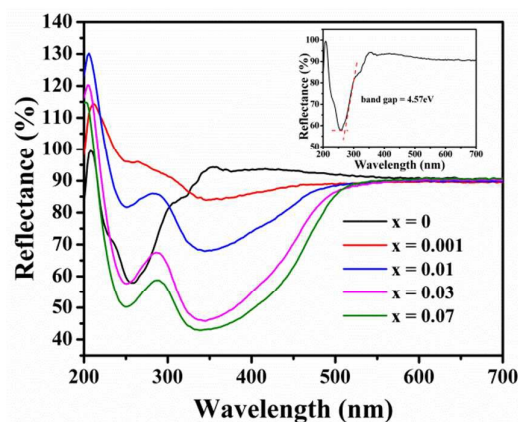
**Fig. 3** Crystal structure of Na<sub>3</sub>LuSi<sub>2</sub>O<sub>7</sub> host.

**Table 2** Selected Na-O bond lengths in the Na<sub>3</sub>LuSi<sub>2</sub>O<sub>7</sub> compound.

Selected atoms	Bond length	Selected atoms	Bond length	Average bond length
Na1-O3	2.557 Å (six)			2.557 Å
Na2-O4	2.248 Å (two)	Na2-O4	2.247 Å	2.2477 Å
Na3-O2	2.508 Å (six)			2.508 Å
Na4-O1	2.354 Å	Na4-O1	2.536 Å	2.387 Å
Na4-O2	2.343 Å	Na4-O3	2.315 Å	

### 3. 2 Diffuse reflection and PL spectra of Eu<sup>2+</sup> doped NLSO phosphor.

The diffuse reflection spectra of un-doped and Eu<sup>2+</sup>-doped Na<sub>3</sub>LuSi<sub>2</sub>O<sub>7</sub> phosphors are displayed in Fig. 6. It is easily seen that the profile of diffuse reflection spectrum of NLSO host is much different from those of Eu<sup>2+</sup> doped NLSO samples, which illustrate the Eu<sup>2+</sup> can be as an effective activator and produce its characteristic excitation and emission spectra properties in this host. Clearly, the un-doped NLSO shows a remarkable drop in reflection around 250 nm. However, there are primary two absorption bands in the range from 200-520 nm, one is over 200-280 nm, which is originated from host, and the more intense one is over the 280-520 nm UV and n-UV range around 350 nm, which is attributed to the

**Fig. 4** Raman spectrum of the representative NLSO host.**Fig. 5** The FT-IR spectra of NLSO host and representative Eu<sup>2+</sup> doped NLSO samples, inset is the structure of [Si<sub>2</sub>O<sub>7</sub>]<sup>6-</sup> group.**Fig. 6** Diffuse reflection spectra of the NLSO:xEu<sup>2+</sup> (x = 0-0.07) samples. Inset is the approximate band gap of the NLSO host.

4f-5d absorption of the Eu<sup>2+</sup> ions and matches well with the excitation spectrum, which will be also discussed below. The absorption intensity is enhanced with increasing Eu<sup>2+</sup> concentration, indicating that the absorption bands in Eu<sup>2+</sup> doped samples derive from Eu<sup>2+</sup> ions. To determine the absorption edge approximately from the obtained diffuse reflectance spectrum of host, the Kubelka-Munk absorption coefficient (K/S) relationship was often used and presented below:<sup>16</sup>

$$F(R) = \frac{K}{S} = \frac{(1-R)^2}{2R} \quad (1)$$

where F(R) is the Kubelka-Munk function, K and S are the absorption and scattering coefficient, respectively, R refers to the measured reflection. The optical band gap energy of NLSO is determined to be 4.57 eV after the linear extrapolation to F(R) = 0 according to the inset of Fig. 6. This is important because of the valence to conduction band transitions of the Na<sub>3</sub>LuSi<sub>2</sub>O<sub>7</sub> host. Fig. 7a shows the PL emission and excitation spectra of NLSO:0.01Eu<sup>2+</sup>. The excitation spectrum monitored at 508 nm contains several broad bands extending from 210 nm to 500 nm centered at about 273, 299, 327 and 365 nm, respectively, which agrees well with the reflection spectrum presented above, indicating effective excitation of the phosphor by the NUV LED chips (350–420 nm) and interesting desire for applications in w-LEDs. The first band may be ascribed to the valence-to-conduction band of the host lattice, while the others can be attributed to the 5d-4f allowed transition of Eu<sup>2+</sup> ion. The emission spectra excited at 327 and 365 nm present identical profiles except for the intensity. They both consist of a wide and asymmetric band with the extent from 420 to 650 nm around 508 nm. The full-width at half-maximum (FWHM) of the PL emission spectrum of is about 82 nm under 365 nm excitation, indicating it covers a broad green-emitting area. The calculated Stokes shift between the excitation peak at 365 nm and emission peak at 508 nm is about 7712 cm<sup>-1</sup>. Considering the four kinds of Na<sup>+</sup> sites for Eu<sup>2+</sup> occupancy, we plot the emission spectrum of NLSO:0.01Eu<sup>2+</sup> under 365 nm excitation and decompose it into four bands by Gaussian fitting in Fig. 7b. As we can see, the four bands are centered at 497 nm, 532 nm, 552 nm and 568 nm with corresponding wavenumber of 20121 cm<sup>-1</sup>, 18797 cm<sup>-1</sup>, 18116 cm<sup>-1</sup> and 17606 cm<sup>-1</sup> in inset of Fig. 7b, respectively. The different

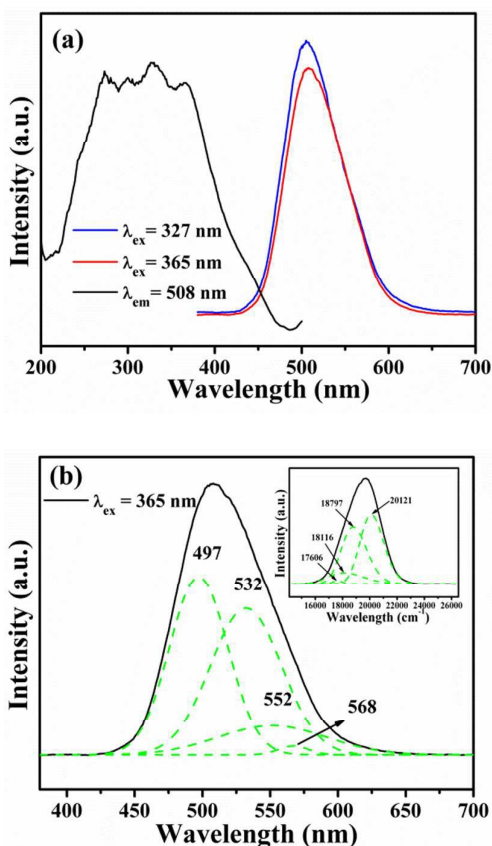


**Fig. 7** (a) PL excitation and emission spectra of NLSO:0.01Eu<sup>2+</sup>. (b) Gaussian fitting into four emission bands from emission spectrum under 365 nm excitation. Inset is the fitting bands with corresponding wavenumbers.

local crystal field environment can be generated when Na<sup>+</sup> are substituted by Eu<sup>2+</sup> ions. In order to understand the derivation of emission peaks by qualitatively analyzing the present experimental result, the theoretical formula suggested by Van Uitert has been used:<sup>17</sup>

$$E = Q \left[ 1 - \left( \frac{V}{4} \right)^{\frac{1}{3}} 10^{-\frac{n \times E_a \times r}{80}} \right] \quad (2)$$

where  $E$  refers to the energy position of the d-band edge for rare earth ions (cm<sup>-1</sup>);  $Q$  represents the energy position of the lower d band edge for the free ions (34000 cm<sup>-1</sup> for Eu<sup>2+</sup> here);  $V$  is the valence of the activator, such as Eu<sup>2+</sup> ion here ( $V = 2$ ); " $E_a$ " is the electron affinity of the anion atoms (in eV) depending on the anion complex type; In addition,  $n$  corresponds to the number of anions in the immediate shell around the active Eu<sup>2+</sup> ion;  $r$  refers to the effective radius of the host cation (Na<sup>+</sup> ion) replaced by the Eu<sup>2+</sup> ion. According to the equation, we can easily conclude that the value of  $E$  is proportional to the two parameters of  $n$  and  $r$ . Consequently, the emission bands around 497, 532, 552 and 568 nm can be assigned to Eu<sup>2+</sup> occupying Na<sup>+</sup> with six, six, four and three oxygen atoms coordination, respectively. Therefore, we need to differentiate the two six-coordination sites. As is known, the different crystal field strengths are produced with different

coordination environments. In this case, the crystal field splitting ( $D_q$ ) can be determined by the following equation:<sup>18</sup>

$$D_q = \frac{1}{6} Z e^2 \frac{r^4}{R^5} \quad (3)$$

where  $D_q$  is a measure of the energy level separation,  $Z$  refers to the anion charge,  $e$  represents the electron charge,  $r$  refers to the radius of the d wave function, and  $R$  corresponds to the bond length. As listed in Table 2 and mentioned above, the average bond length of Na3-O2 is much longer than that of Na3-O3, which illustrated that the  $D_q$  of Na1-O3 hexahedron is more intense than that of Na1-O3 according to the crystal field theory.<sup>18a</sup> This analysis infers that the band with longer wavelength originates from Na1-O3, corresponding to the band around 532 nm when Eu<sup>2+</sup> occupy Na<sup>+</sup> lattice site here.

### 3.3 PL emission spectra and lifetimes of NLSO:Eu<sup>2+</sup> phosphors as a function of Eu<sup>2+</sup> concentration

Fig. 8a shows the emission spectra on the Eu<sup>2+</sup> concentration  $x$  upon 365 nm UV excitation, from which we can see the profiles of emission spectra are similar to each other with the increase of Eu<sup>2+</sup> concentration. Moreover, the emission intensity of Eu<sup>2+</sup> first increased until the maximum at a Eu<sup>2+</sup> concentration of 0.03, beyond which the emission intensity began to decrease with further concentration. It can be concluded that the optimum doping concentration  $x$  value of Eu<sup>2+</sup> is 0.01, as depicted in Fig. 8b. After critical value, the emission intensity decreased critically attributed to the concentration quenching effect. It is accepted that energy transfer among Eu<sup>2+</sup> ions mainly results in the concentration quenching, and the probability of this increases with increasing doping Eu<sup>2+</sup> concentration until the energy is consumed. The lifetime of Eu<sup>2+</sup> ion can be assessed by the simple equation which can be copied below:<sup>19</sup>

$$\tau = \int_0^{\infty} I(t) dt \quad (4)$$

where  $\tau$  refers to calculated lifetime value, and  $I(t)$  is the normalized intensity of decay curves. According to the equation (4) and decay curves in Fig. 8c, the values of different Eu<sup>2+</sup>-doped samples were determined to be 0.633, 0.546, 0.511, 0.497, 0.385, 0.344, 0.299 and 0.285  $\mu$ s corresponding to  $x = 0.0005, 0.001, 0.005, 0.01, 0.02, 0.03, 0.05$  and  $0.07$ . It is also reasonable that the decay times decrease monotonously with the increase of Eu<sup>2+</sup> concentration. Therefore, the monotonous decrease of decay times can be obviously found in Eu<sup>2+</sup> doped NLSO samples with the increase of Eu<sup>2+</sup> concentration. To further ascertain the energy transfer mechanism in NLSO:Eu<sup>2+</sup> samples, it needs to know the critical distance ( $R_c$ ) between activators such as Eu<sup>2+</sup> here. The calculated formula of  $R_c$  has been proposed by Blasse earlier:<sup>20</sup>

$$R_c \approx 2 \left[ \frac{3V}{4\pi X_c N} \right]^{-1/3} \quad (5)$$

where  $V$  corresponds to the volume of the unit cell,  $N$  is the number of available sites for the dopant in the unit cell, and  $X_c$  refers to the critical concentration of dopant ions. For the NLSO host,  $N = 24$ ,  $V = 1046.23 \text{ \AA}^3$ , and  $X_c$  is 0.01 for Eu<sup>2+</sup>; Accordingly, the critical distance ( $R_c$ ) was estimated to be about 20.27  $\text{\AA}$ .

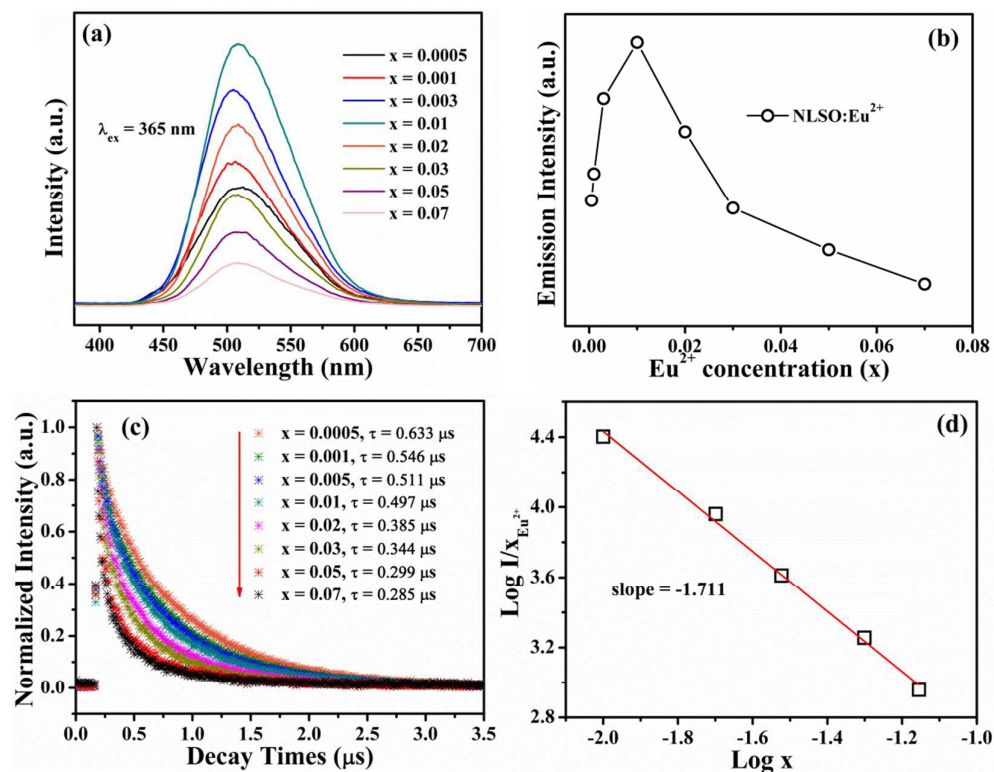


**Fig. 8** (a) PL emission spectra of NLSO:xEu<sup>2+</sup> ( $x = 0.0005-0.07$ ) upon 365 nm excitation. (b) Variations of emission intensity with increasing Eu<sup>2+</sup> concentration  $x$  in NLSO:xEu<sup>2+</sup> phosphors. (c) Decay times of NLSO:Eu<sup>2+</sup> as a function of Eu<sup>2+</sup> concentration  $x$  (monitored at 508 nm and excited at 330 nm). (d) Linear fitting of  $\log(x)$  versus  $\log(I/x)$  in various NLSO:xEu<sup>2+</sup> phosphors beyond the concentration quenching ( $x > 0.01$ ).

Generally, exchange interaction, radiation reabsorption, and electric multipolar interaction are responsible for non-radiative energy transfer mechanisms. We can easily infer that the little possibility of exchange interaction since the exchange interaction is predominant only for about 5 Å which is far less than the result obtained 20.27 Å above.<sup>21</sup> The mechanism of radiation reabsorption occurs when the fluorescence and absorption spectra are widely overlapping, which is not likely to take place in this case. Accordingly, we can infer the energy transfer mechanism between Eu<sup>2+</sup> ions is effective via electric multipolar interaction. According to the calculated equation by Dexter and Van Uitert, which can be delivered as follow:<sup>22</sup>

$$\frac{I}{x} = [1 + \beta(x)^{\theta/3}]^{-1} \quad (6)$$

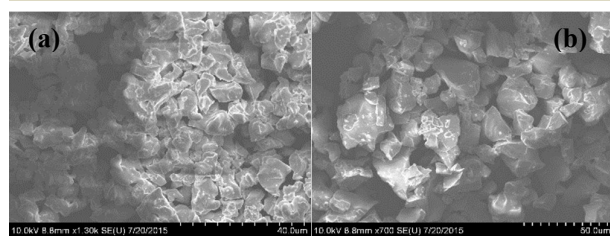


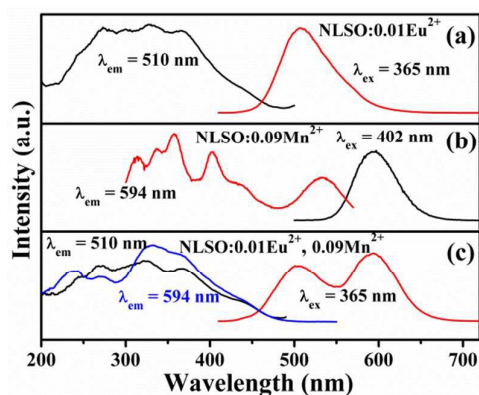
**Fig. 9** SEM image of the selected NLSO:0.01Eu<sup>2+</sup> (a) and NLSO:0.01Eu<sup>2+</sup>,0.09Mn<sup>2+</sup> (b) samples.

where  $I$  refers to the emission intensity,  $x$  represents the activator ion concentration, and  $\theta$  represents a constant for the fixed matrix under the same excitation conditions. The type of energy transfer mechanism of electric multipolar interaction can be evaluated by analyzing the constant  $\theta$  from this formula. The value of  $\theta = 6, 8$  and  $10$  correspond to electric dipole-dipole, dipole-quadrupole and quadrupole-quadrupole interactions, respectively. The dependence of  $I/x$  on  $x$  on a logarithmic scale was illustrated in Fig. 8d to determine the value of  $\theta$ . An approximate linear relation between  $\log(I/x\text{Eu}^{2+})$  and  $\log(x\text{Eu}^{2+})$  can be found and the slope of fitted straight line is equal to  $-1.711 = -\theta/3$ , consequently, the  $\theta = 5.133$  is approximately as 6, illustrating the dipole-dipole interaction was responsible for the energy transfer mechanism between Eu<sup>2+</sup> in NLSO:Eu<sup>2+</sup> phosphors.

Fig. 9 shows the microstructure and morphology of the representative NLSO:0.01Eu<sup>2+</sup> and NLSO:0.01Eu<sup>2+</sup>,0.09Mn<sup>2+</sup> samples, which were determined by SEM measurement. It is observed that the particles have the irregular morphology and some grains have aggregated together, however, they can be assessed with the size from about 4 to 25 μm, which is believed that such morphology will be very helpful in practical fabrication of white LEDs devices.

### 3.4 Energy transfer properties in Eu<sup>2+</sup>, Mn<sup>2+</sup> co-doped NLSO phosphors

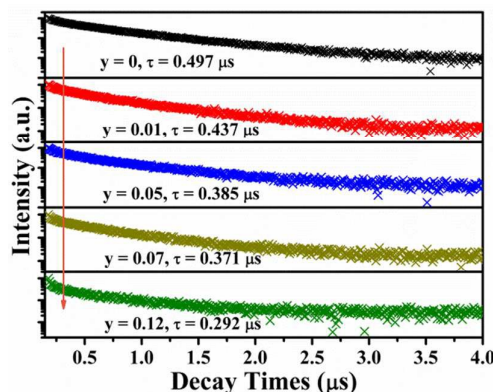
Sections a and b in Fig. 10 show the PL excitation and emission spectra of NLSO:0.01Eu<sup>2+</sup>, NLSO:0.09Mn<sup>2+</sup> and NLSO:0.01Eu<sup>2+</sup>,



**Fig. 10** PL excitation and emission spectra of NLSO:0.01Eu<sup>2+</sup> (a), NLSO:0.09Mn<sup>2+</sup> (b), and NLSO:0.01Eu<sup>2+</sup>, 0.09Mn<sup>2+</sup> (c) phosphors.

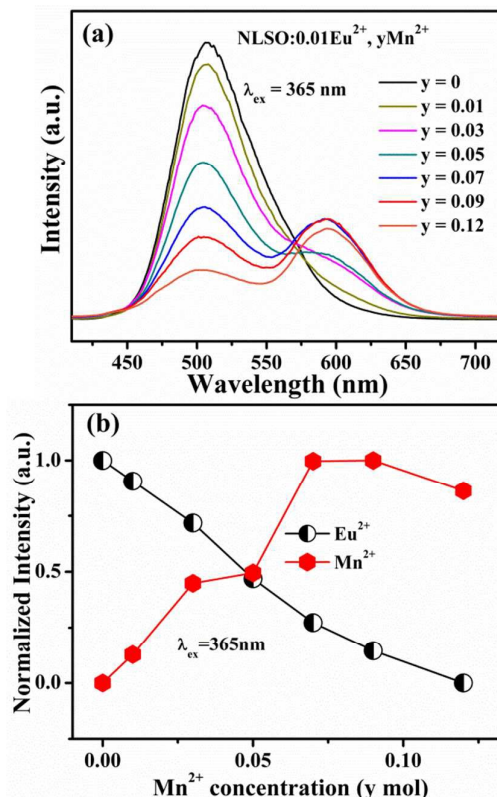
0.09Mn<sup>2+</sup> phosphors. The emission spectrum of NLSO:0.09Mn<sup>2+</sup> presents a broad band extending from 530 to 650 nm centered at 594 nm upon 402 nm excitation in Fig. 10b, which is originated from the <sup>4</sup>T<sub>1g</sub>(G)-<sup>6</sup>A<sub>1g</sub>(S) spin-forbidden transition of Mn<sup>2+</sup> ions. The occurrence of several peaks from 320 to 550 nm owes to the Mn<sup>2+</sup> ion 4f-4f transition in the excitation spectrum of NLSO:0.09Mn<sup>2+</sup> monitored at 594 nm. It is obvious that there exists the overlap of Eu<sup>2+</sup> emission and Mn<sup>2+</sup> excitation in the range of 500 to 570 nm. Therefore, the resonance type energy transfer probability from Eu<sup>2+</sup> to Mn<sup>2+</sup> ions can be inferred from it. Besides, the similar excitation spectra monitored at 508 and 594 nm in Fig. 10c can be used to certify the energy transfer from Eu<sup>2+</sup> to Mn<sup>2+</sup> ions. In addition, the emission spectrum excited at 365 nm covers both the Eu<sup>2+</sup> and Mn<sup>2+</sup> emission bands, therefore, the tunable color would like to be produced via adjusting the concentration ratio of Eu<sup>2+</sup>/Mn<sup>2+</sup> under UV excitation. In order to further testify the energy transfer from Eu<sup>2+</sup> to Mn<sup>2+</sup> ion in NLSO:0.01Eu<sup>2+</sup>, yMn<sup>2+</sup> (y = 0-0.12) phosphors, we plotted the decay curves monitored at 508 nm excited at 330 nm and calculated the decay lifetimes approximately from them in Fig. 11. The decay times of Eu<sup>2+</sup> ions in Eu<sup>2+</sup>, Mn<sup>2+</sup> co-doped NLSO samples are determined to be 0.497, 0.437, 0.385, 0.371 and 0.292 μs corresponding to the Mn<sup>2+</sup> concentration y = 0, 0.01, 0.05, 0.07 and 0.12 in NLSO:0.01Eu<sup>2+</sup>, yMn<sup>2+</sup> phosphors according to the equation (4). It is clear that the decrease of Eu<sup>2+</sup> decay lifetimes occurs with increasing Mn<sup>2+</sup> concentration, which supplies the confirmation of energy transfer from Eu<sup>2+</sup> to Mn<sup>2+</sup> ions again.

Fig. 12a shows the PL emission spectra excited at 365 nm for NLSO:0.01Eu<sup>2+</sup>, yMn<sup>2+</sup> (y = 0-0.12) phosphors on Mn<sup>2+</sup> doping content. One can find the Eu<sup>2+</sup> emission intensity drops monotonously, while the emission intensity of Mn<sup>2+</sup> increases gradually until the Mn<sup>2+</sup> concentration y = 0.09 in NLSO:0.01Eu<sup>2+</sup>, yMn<sup>2+</sup> phosphors with the increase of Mn<sup>2+</sup> content, as displayed in Fig. 12b. The decline of Mn<sup>2+</sup> emission intensity with further Mn<sup>2+</sup> concentration can be ascribed to the concentration quenching effect. This result gives a further certification of energy transfer from Eu<sup>2+</sup> to Mn<sup>2+</sup> ions in NLSO:0.01Eu<sup>2+</sup>, yMn<sup>2+</sup> samples. Based on the energy transfer from Eu<sup>2+</sup> to Mn<sup>2+</sup> ion and the analysis of emission spectra of NLSO:0.01Eu<sup>2+</sup>, yMn<sup>2+</sup> samples, the emission color can be tuned from green to yellowish orange with the CIE chromaticity coordinates from 1(0.212, 0.544) to 7(0.428, 0.432) corresponding to y = 0 to 0.12 under 365 nm excitation,



**Fig. 11** Decay curves and calculated lifetimes of Eu<sup>2+</sup> in representative samples NLSO:0.01Eu<sup>2+</sup>, yMn<sup>2+</sup> (monitored at 508 nm excited at 330 nm).

respectively, which are calculated and listed in Table 3. The detailed emission colors and CIE coordinate diagram have been presented in Fig. 13a. The absolute quantum yields for NLSO:0.01Eu<sup>2+</sup>, yMn<sup>2+</sup> phosphors excited at 365 nm UV are also listed in Table 3, which shows the maximum value 51.5% for NLSO:0.01Eu<sup>2+</sup>, 0.12Mn<sup>2+</sup>. Moreover, simple energy level scheme of energy transfer



**Fig. 12** (a) Variation of PL emission spectra for NLSO:0.01Eu<sup>2+</sup>, yMn<sup>2+</sup> (y = 0-0.12) phosphors as a function of Mn<sup>2+</sup> doping content upon 365 nm excitation. (b) Dependence of normalized emission intensity of Eu<sup>2+</sup> and Mn<sup>2+</sup> in NLSO:0.01Eu<sup>2+</sup>, yMn<sup>2+</sup> phosphors on Mn<sup>2+</sup> concentration.

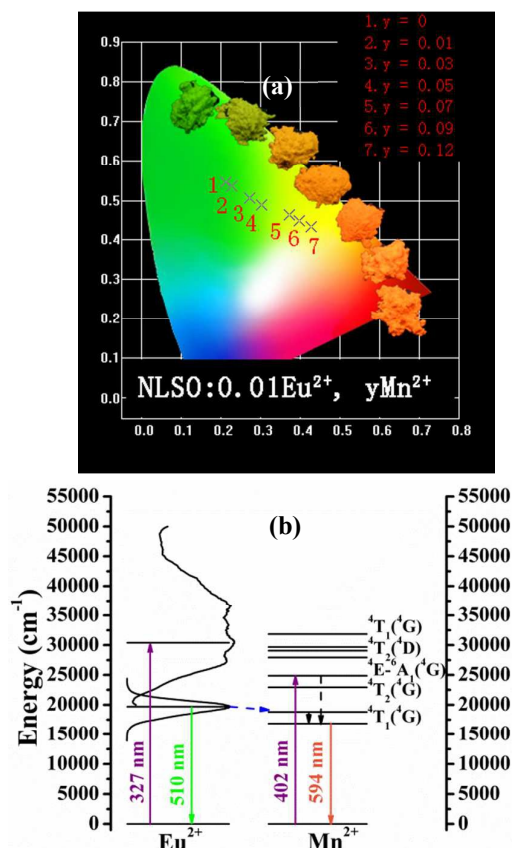


**Fig. 13** (a) CIE chromaticity coordinate diagram of the as-prepared sample NLSO:0.01Eu<sup>2+</sup>,yMn<sup>2+</sup> and the corresponding digital photos under 365 nm UV lamp excitation. (b) Simple energy level scheme of energy transfer in NLSO:Eu<sup>2+</sup>,Mn<sup>2+</sup> phosphors.

in NLSO:Eu<sup>2+</sup>,Mn<sup>2+</sup> is displayed in Fig. 13b, corresponding to the excitation and emission energy of Eu<sup>2+</sup> and Mn<sup>2+</sup> ions, and the energy transfer process from Eu<sup>2+</sup> to Mn<sup>2+</sup> ions is presented clearly. As to this host, the energy transfer efficiency ( $\eta_T$ ) from Eu<sup>2+</sup> to Mn<sup>2+</sup> ions can be approximately estimated using following equation:<sup>23</sup>

$$\eta_T = 1 - \frac{I_S}{I_{S0}} \quad (7)$$

where  $\eta_T$  represents the energy transfer efficiency,  $I_{S0}$  and  $I_S$  are the luminescence intensity of Eu<sup>2+</sup> ions without and with the existence of Mn<sup>2+</sup> ions, respectively. Fig. 14 shows the dependence of approximately calculated values  $\eta_T$  on Mn<sup>2+</sup> concentration. The monotonous raise of it appears with constant increase in Mn<sup>2+</sup> concentration while the increasing rate falls because the stationary Eu<sup>2+</sup> concentration limits the energy transfer from Eu<sup>2+</sup> to Mn<sup>2+</sup> ions.

As described in section 3.3, for this host, the  $R_c$  is calculated to be 10.60 Å by using the equation 4, where the different  $X_c$  value is defined as the critical concentration of dopant ions (total concentration of Eu<sup>2+</sup> and Mn<sup>2+</sup>, approximately 0.07), that is, at which the luminescence intensity of Eu<sup>2+</sup> is half of that in the sample without Mn<sup>2+</sup>. The result indicates the electric multipolar interaction would like to take place for energy transfer between Eu<sup>2+</sup> and Mn<sup>2+</sup> in this host. On account of Dexter's energy transfer

**Table 3** Variations of quantum yields and CIE chromaticity coordinates (x, y) for NLSO:0.01Eu<sup>2+</sup>,yMn<sup>2+</sup> phosphors excited at 365 nm UV.

Sample no.	Mn <sup>2+</sup> concentration (y)	CIE chromaticity coordinates (x, y)	QY (%)
1	0	(0.212, 0.544)	44.5
2	0.01	(0.228, 0.534)	37.8
3	0.03	(0.273, 0.506)	43.2
4	0.05	(0.303, 0.487)	50.9
5	0.07	(0.372, 0.462)	45.5
6	0.09	(0.397, 0.448)	49.4
7	0.12	(0.428, 0.432)	51.5

formula of multipolar interaction, the following relationship can be obtained:<sup>24</sup>

$$\frac{\eta_{S0}}{\eta_S} \propto C^{\alpha/3} \quad (8)$$

where  $\eta_{S0}$  and  $\eta_S$  refer to the luminescence quantum efficiencies of the Eu<sup>2+</sup> ions with the absence and presence of the Mn<sup>2+</sup> ions, respectively.  $C$  represents the sum of the Eu<sup>2+</sup> and Mn<sup>2+</sup> ions concentrations. The values  $\alpha = 6, 8$  and  $10$  correspond to dipole-dipole, dipole-quadrupole, and quadrupole-quadrupole interactions, respectively. However, the  $\eta_{S0}/\eta_S$  is difficult to be gained and therefore it can be evaluated instead by the  $I_{S0}/I_S$ , where  $I_{S0}$  and  $I_S$  stand for the luminescence intensity of the Eu<sup>2+</sup> ions without and with the Mn<sup>2+</sup> ions, respectively, therefore, the above equation can be substituted as follow:

$$\frac{I_{S0}}{I_S} \propto C^{\alpha/3} \quad (9)$$

The relationship between  $I_{S0}/I_S$  and  $C^{\alpha/3}$  based on the above equation are plotted in Fig. 15. One can find that the  $R^2$  of the linear fitting in Fig. 15b is more than those in Fig. 15a and c, which indicates that this relationship is the best linear behavior when  $\alpha = 8$ . Therefore, the dipole-quadrupole mechanism can be responsible for the energy transfer from Eu<sup>2+</sup> to Mn<sup>2+</sup> ions. Considering the dipole-quadrupole interaction, the  $R_c$  value also can be obtained

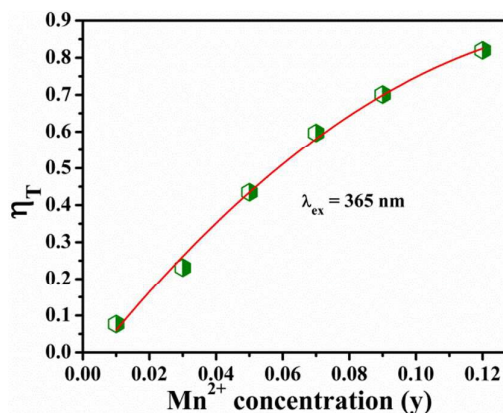


**Fig. 14** Dependence of energy transfer efficiency( $\eta_T$ ) on Mn<sup>2+</sup> concentration.

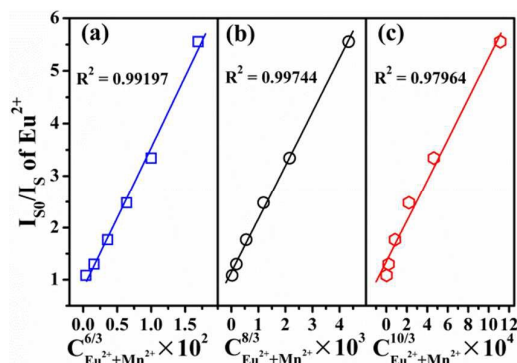


**Fig. 15** Dependence of  $I_{50}/I_5$  of  $\text{Eu}^{2+}$  on  $C^{6/3}$  (a),  $C^{8/3}$  (b), and  $C^{10/3}$  (c) in  $\text{NLSO}:\text{Eu}^{2+},\text{Mn}^{2+}$  phosphors.

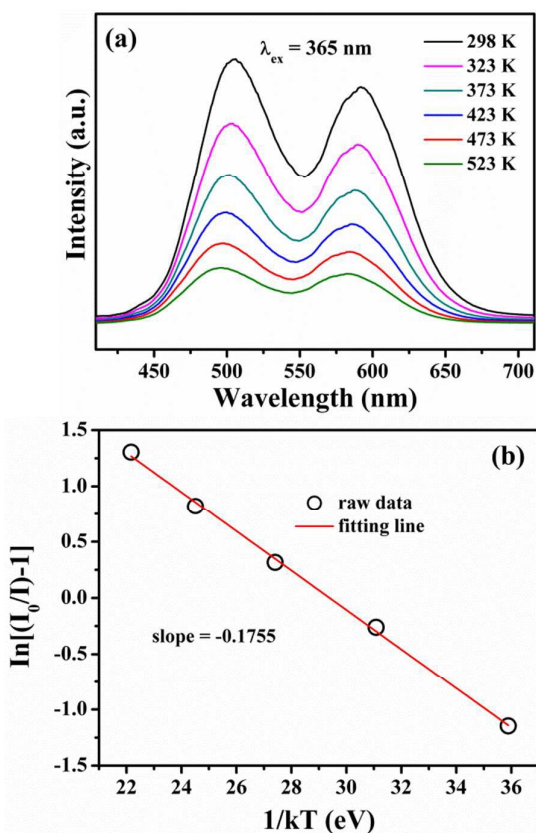


**Fig. 16** (a) Temperature-dependent PL spectra of  $\text{NLSO}:\text{0.01Eu}^{2+},\text{0.07Mn}^{2+}$  phosphor; inset shows the integrated intensity vs. temperature ( $\lambda_{\text{ex}} = 365 \text{ nm}$ ). (b) The relationship of  $\ln(I_0/I-1)$  versus  $1/kT$  activation energy graph for thermal quenching for  $\text{NLSO}:\text{0.01Eu}^{2+},\text{0.07Mn}^{2+}$  sample.

through spectral overlap way which has the expression given by following equation:<sup>25</sup>

$$R_c^8 = 3.024 \times 10^{12} \lambda_s^2 f_q \int f_s(E) f_A(E) / E^4 dE \quad (10)$$

where  $f_q = 10^{-10}$  is the oscillator strength of  $\text{Mn}^{2+}$  dipole and quadrupole electrical absorption transitions;  $\lambda_s = 5080 \text{ \AA}$  is the wavelength of strongest intensity of  $\text{Eu}^{2+}$ ;  $E$  is the energy involved in the transfer (in eV);  $\int f_s(E) f_A(E) / E^4 dE$  represents the spectral overlap

between the normalized shapes of the  $\text{Eu}^{2+}$  emission  $f_s(E)$  and the  $\text{Mn}^{2+}$  excitation  $f_A(E)$ , and in our condition it is calculated to be about  $0.0925 \text{ eV}^{-5}$ . Accordingly, the value of  $R_c$  is determined to be  $12.80 \text{ \AA}$ , which approximately agrees with that obtained by concentration quenching method above. The result can further demonstrate the electric dipole-quadrupole interaction dominates the energy transfer mechanism from  $\text{Eu}^{2+}$  to  $\text{Mn}^{2+}$  ions in this host.

### 3.5 Thermal-dependent photoluminescence properties

Generally, the thermal stability is a key parameter for phosphors to be considered in the fabrication of LEDs. On the basis of this situation, we have investigated the thermal quenching property of the representative  $\text{NLSO}:\text{0.01Eu}^{2+},\text{0.07Mn}^{2+}$  sample. It can be seen that the  $\text{NLSO}:\text{0.01Eu}^{2+},\text{0.07Mn}^{2+}$  phosphor demonstrates a constant decrease of PL intensity and relatively poor thermal stability with increasing temperature. The PL intensity of  $\text{NLSO}:\text{0.01Eu}^{2+},\text{0.07Mn}^{2+}$  phosphor at  $150 \text{ }^\circ\text{C}$  is about 42 % of its initial value at room temperature under 365 nm excitation, as depicted in the Fig. 16a, however, the relative intensity can be acceptable. It is believed that the reason for the decrease of emission intensity is attributed to the thermal quenching via the thermal activation through the crossing point between the ground and the excited states.<sup>26</sup> Additionally, a minor blue shift can be found in the emission wavelengths with the increase of temperature, which can be explained by the thermally active phonon-assisted excitation from the excited states of the lower-energy to the higher-energy emission bands in the excited states of  $\text{Eu}^{2+}$  and  $\text{Mn}^{2+}$ .<sup>27</sup> The Arrhenius equation expressing the relationship between temperature and luminescence intensity was used to understand the thermal quenching phenomenon and determine the activation energy ( $E_a$ ), which can be illustrated below:<sup>28</sup>

$$\ln\left(\frac{I_0}{I}\right) = \ln A - \frac{E_a}{kT} \quad (11)$$

where  $I_0$  and  $I$  are the integral intensity at the room temperature and certain given temperature, respectively.  $A$  is a constant,  $E_a$  is the activation energy,  $T$  refers to the temperature (K) and  $k$  is the Boltzmann constant ( $8.626 \times 10^{-5} \text{ eV}$ ). Fig. 16b plots the relationship of  $\ln(I_0/I-1)$  versus  $1/kT$  activation energy graph for thermal quenching of  $\text{NLSO}:\text{0.01Eu}^{2+},\text{0.07Mn}^{2+}$  phosphor, which presents the linear fitting with the slope of  $-0.1755$ , therefore, the activation energy  $E_a$  is estimated to be  $0.1755 \text{ eV}$ , which is a little smaller than that in similar systems  $\text{NaCaY}(\text{PO}_4)_2:\text{Eu}^{2+},\text{Mn}^{2+}$  ( $0.201 \text{ eV}$ ) and  $\text{Ca}_{14}\text{Mg}_2(\text{SiO}_4)_8:\text{Eu}^{2+},\text{Mn}^{2+}$  ( $0.205 \text{ eV}$ ).<sup>29</sup> A larger  $E_a$  indicates better thermal quenching properties, thus this kind of  $\text{Eu}^{2+}, \text{Mn}^{2+}$  co-doped NLSO samples has a little worse thermal properties than them.

## 4 Conclusions

A series of pure  $\text{Eu}^{2+}$ ,  $\text{Mn}^{2+}$ -doped NLSO phosphors have been prepared via the high-temperature solid-state reaction route. The  $\text{Eu}^{2+}$  singly doped NLSO phosphors present intense green emission under UV excitation. The site occupancy of  $\text{Eu}^{2+}$  in the NLSO structure has been analyzed in detail. The tunable color from green to yellowish-orange has been generated based on the energy transfer from  $\text{Eu}^{2+}$  to  $\text{Mn}^{2+}$  ions when  $\text{Mn}^{2+}$  are added into the  $\text{Eu}^{2+}$ -

doped NLSO samples under UV excitation. The energy transfer from  $\text{Eu}^{2+}$  to  $\text{Mn}^{2+}$  can be certified via the similar excitation spectra of  $\text{Eu}^{2+}$  and  $\text{Mn}^{2+}$  emissions and the decreases of  $\text{Eu}^{2+}$  decay times and emission intensity with the increase of  $\text{Mn}^{2+}$  concentration in NLSO: $\text{Eu}^{2+}$ , $\text{Mn}^{2+}$  samples. The energy transfer mechanism from  $\text{Eu}^{2+}$  to  $\text{Mn}^{2+}$  has been demonstrated to be dipole-quadrupole interaction. Additionally, the quantum yields, CIE values, the typical morphology and PL thermal quenching properties of the selected NLSO: $\text{Eu}^{2+}$ , $\text{Mn}^{2+}$  phosphors have been investigated in detail. The results above indicate that NLSO: $\text{Eu}^{2+}$ , $\text{Mn}^{2+}$  can be as a candidate for the green-yellowish-orange component in UV-excited w-LEDs.

## Acknowledgements

This project is financially supported by the Scientific and Technological Department of Jilin Province (Grant No. 20150520029JH), National Natural Science Foundation of China (NSFC Grants 51472234, 51172227, 91433110), National Basic Research Program of China (Grants 2014CB643803), and Joint Funds of the National Natural Science Foundation of China (Grant U13012038).

## References

- (a) X. Piao, K. Machida, T. Horikawa, H. Hanzawa, Y. Shimomura and N. Kijima, *Chem. Mater.*, 2007, **19**, 4592; (b) Y.-C. Chiu, W.-R. Liu, C.-K. Chang, C.-C. Liao, Y.-T. Yeh, S.-M. Jang and T.-M. Chen, *J. Mater. Chem.*, 2010, **20**, 1755; (c) W. B. Im, Y. I. Kim, N. N. Fellows, H. Masui, G. A. Hirata, S. P. Den and B. R. Seshadri, *Appl. Phys. Lett.*, 2008, **93**, 091905; (d) S. Ye, F. Xiao, Y. X. Pan, Y. Y. Ma and Q. Y. Zhang, *Mater. Sci. Eng. R*, 2010, **71**, 1.
- (a) W. Lu, Z. Hao, X. Zhang, Y. Luo, X. Wang and J. Zhang, *Inorg. Chem.*, 2011, **50**, 7846; (b) W. R. Liu, C. H. Huang, C. W. Yeh, J. C. Tsai, Y. C. Chiu, Y. T. Yeh and R. S. Liu, *Inorg. Chem.*, 2012, **51**, 9636; (c) A. A. Setlur, W. J. Heward, Y. Gao, A. M. Srivastava, R. G. Chandran and M. V. Shankar, *Chem. Mater.*, 2006, **18**, 3314.
- (a) G. Anoop, D. W. Lee, D. W. Suh, S. L. Wu, K. M. Ok and J. S. Yoo, *J. Mater. Chem. C*, 2013, **1**, 4705; (b) R. J. Xie, N. Hirosaki, K. Sakuma, Y. Yamamoto and M. Mitomo, *Appl. Phys. Lett.*, 2004, **84**, 5404.
- (a) X. Gong, J. Huang, Y. Chen, Y. Lin, Z. Luo and Y. Huang, *Inorg. Chem.*, 2014, **53**, 6607; (b) Q. Wu, X. Wang, Z. Zhao, C. Wang, Y. Li, A. Mao and Y. Wang, *J. Mater. Chem. C*, 2014, **2**, 7731. (c) G. Lee, J. Y. Han, W. B. Im, S. H. Cheong and D. Y. Jeon, *Inorg. Chem.*, 2012, **51**, 10688; (d) R. Yu, H. Li, H. Ma, C. Wang and H. Wang, *J. Am. Ceram. Soc.*, 2014, **1**, 1. (e) W. Li, R.-J. Xie, T. Zhou, L. Liu and Y. Zhu, *Dalton Trans.*, 2014, **43**, 6132.
- (a) P. Li, Z. Wang, Z. Yang and Q. Guo, *J. Mater. Chem. C*, 2014, **2**, 7823; (b) M. Zhang, Y. Liang, W. Huang, Z. Xia, D. Yu, Y. Lan, G. Li and W. Zhou, *Mater. Res. Bull.*, 2014, **57**, 231; (c) H. Liu, L. Liao and Z. Xia, *RSC Adv.*, 2014, **4**, 7288; (d) Z. Chen, J. H. Zhang, S. Chen, M. Y. Lin, C. Q. He, G. D. Xu, M. M. Wang, X. F. Yu, J. Q. Zou and K. Guo, *J. Alloys Compd.*, 2015, **632**, 756.
- W. Lv, Y. Jia, Q. Zhao, M. Jiao, B. Shao, W. Lü and H. You, *RSC Adv.*, 2014, **4**, 7588.
- (a) C.-H. Huang, W.-R. Liu, T.-S. Chan and Y.-T. Lai, *Dalton Trans.*, 2014, **43**, 7917; (b) J. Yan, . Ning, Y. Huang, C. Liu, D. Hou, B. Zhang, Y. Huang, Y. Tao and H. Liang, *J. Mater. Chem. C*, 2014, **2**, 8328; (c) J. Wang, Y. Huang, X. Wang, L. Qin and H. J. Seo, *Mater. Res. Bull.*, 2014, **55**, 126; (d) Z. Ci, Q. Sun, S. Qin, M. Sun, X. Jiang, X. Zhang and Y. Wang, *Phys. Chem. Chem. Phys.*, 2014, **16**, 11597; (e) X. Yu, L. Zhang, X. Xu, T. Wang, H. Yu, T. Jiang, Q. Jiao, Z. Yang, D. Zhou and J. Qiu, *J. Lumin.*, 2014, **145**, 114.
- (a) Z. Xia, J. Zhou and Z. Mao, *J. Mater. Chem. C*, 2013, **1**, 5917; (b) C. Liu, Z. Xia, Z. Lian, J. Zhou and Q. Yan, *J. Mater. Chem. C*, 2013, **1**, 7139; (c) S. Ray, Y.-C. Fang and T.-M. Chen, *RSC Adv.*, 2013, **3**, 16387.
- H. Ni, H. Liang, M. Xie, W. Chen, Q. Su, Y. Tao, Y. Huang and Z. Gao, *J. Electrochem. Soc.*, 2012, **159**, J43.
- R. A. Tamazyan, Y. A. Malinovskii, M. I. Sirota and V. I. Simonov, *Kristallografiya*, 1988, **33**, 1128.
- (a) J.-L. You, G.-C. Jiang, H.-Y. Hou, H. Chen, Y.-Q. Wu and K.-D. Xu, *J. Raman Spectrosc.*, 2005, **36**, 237; (b) M. Akaogi, N. L. Ross, P. McMillan and A. Navrotsky, *Am. Mineral.*, 1984, **69** (5-6), 499.
- (a) P. McMillan, *Am. Mineral.*, 1984, **69**, 622; (b) R. L. Frost, J. M. Bouzaid and B. J. Reddy, *Polyhedron*, 2007, **26**, 2405.
- (a) S. K. Sharma, B. Simons and H. S. Yoder Jr., *Am. Mineral.*, 1983, **68**, 1113; (b) M. Gabelica-Robert, *J. Mol. Struct.*, 1982, **79**, 255; (c) M. Wierzbicka-Wieczorek, C. Lenz, G. Giester, *Eur. J. Inorg. Chem.*, 2013, **19**, 3405.
- E. V. Galuskin, F. Gfeller, V. B. Savelyeva, T. Armbruster, B. Lazic, I. O. Galuskina, D. M. Tobbens, A. E. Zadov, P. Dzierzanowski, N. NPertsev and V. M. Gazeev, *Am. Mineral.*, 2012, **97**, 503.
- (a) G. Socrates, *Infrared and Raman Characteristic Group Frequencies Tables and Charts*, John Wiley & Sons, West Sussex, England, 2001; (b) A. S. Luyt, M. D. Dramicanin, Z. Antic and V. Djokovic, *Polym. Test.*, 2009, **28**, 348; (c) M. A. Mickens and Z. Assefa, *J. Lumin.*, 2014, **145**, 498.
- (a) X. Chen, Z. Xia and Q. Liu, *Dalton Trans.*, 2014, **43**, 13370; (b) C. H. Huang and T. M. Chen, *Inorg. Chem.*, 2011, **50**, 5725.
- (a) K. Li, D. Geng, M. Shang, Y. Zhang, H. Lian and J. Lin, *J. Phys. Chem. C*, 2014, **118**, 11026; (b) L. G. Van Uitert, *J. Lumin.*, 1984, **29**, 1.
- (a) M. Que, Z. Ci, Y. Wang, G. Zhu, S. Xin, Y. Shi and Q. Wang, *CrystEngComm.*, 2013, **15**, 6389; (b) P. D. Rack and P. H. Holloway, *Mater. Sci. Eng. R*, 1998, **21**, 171.
- N. Guo, Y. Jia, W. Lü, W. Lv, Q. Zhao, M. Jiao, B. Shao and H. You, *Dalton Trans.*, 2013, **42**, 5649.
- G. Blasse, *J. Solid State Chem.*, 1986, **62**, 207.
- (a) W.-R. Liu, C.-H. Huang, C.-P. Wu, Y.-C. Chiu, Y.-T. Yeh and T.-M. Chen, *J. Mater. Chem.*, 2011, **21**, 6869; (b) G. Blasse, *Phys. Lett. A*, 1969, **28**, 444.
- (a) L. G. Van Uitert, *J. Electrochem. Soc.*, 1967, **114**, 1048; (b) D. L. Dexter, *J. Chem. Phys.*, 1953, **21**(5), 836.
- (a) P. I. Paulose, G. Jose, V. Thomas, N. V. Unnikrishnan and M. K. R. Warriar, *J. Phys. Chem. Solids*, 2003, **64**, 841; (b) N. Xie, J. Liu, Y. Huang, S. Kim and H. J. Seo, *Ceram. Inter.*, 2012, **38**, 1489.
- D. L. Dexter and J. H. Schulman, *J. Chem. Phys.*, 1954, **22**, 1063.
- (a) D. Wen, Z. Dong, J. Shi, M. Gong and M. Wu, *ECS J. Solid State Sci. Tech.*, 2013, **2**, R178; (b) J. Chen, Y. Liu, M. Fang and Z. Huang, *Inorg. Chem.*, 2014, **53**, 11396.
- (a) J. S. Kim, Y. H. Park, S. M. Kim, J. C. Choi and H. L. Park, *Solid State Commun.*, 2005, **133**, 445; (b) D. Hsu and J. L. Skinner, *J. Chem. Phys.*, 1984, **81**, 5471.
- (a) Z. Zhao, Z. Yang, Y. Shi, C. Wang, B. Liu, G. Zhu and Y. Wang, *J. Mater. Chem. C*, 2013, **1**, 1407; (b) J. Ruan, R. J. Xie, N. Hirosaki and T. Takeda, *J. Am. Ceram. Soc.*, 2011, **94**, 536.
- (a) X. Zhao, L. Fan, T. Yu, Z. Li and Z. Zou, *Opt. Exp.*, 2013, **21**, 31661; (b) E. Pavitra and J. S. Yu, *Ceram. Inter.*, 2013, **39**, 1029; (c) R. J. Xie and N. Hirosaki, *Appl. Phys. Lett.*, 2007, **90**, 191101.
- (a) W.-R. Liu and P.-C. Lin, *Opt. Exp.*, 2014, **22**, A446; (b) K. H. Lee, S. Choi and H.-K. Jung, W. B. Im, *Acta Mater.*, 2012, **60**, 5783.

## Graphic Abstract

A series of green-yellowish-orange-emitting  $\text{Eu}^{2+}$ ,  $\text{Mn}^{2+}$ -doped  $\text{Na}_3\text{LuSi}_2\text{O}_7$  (NLSO) phosphors synthesized via the high-temperature solid state reaction process have been investigated in detail.

